Environmental Science & Technology

Critical Review

Cite This: Environ. Sci. Technol. 2019, 53, 3366−3378

pubs.acs.org/est

Energy Efficiency of Capacitive Deionization

Li Wang,[†] J. E. Dykstra,[‡] and Shihong Lin*[,†,§]

[†]Department of Civil and Environmental Engineering, Vanderbilt University, Nashville, Tennessee 37235-1831, United States

[‡]Department of Environmental Technology, Wageningen University, Bornse Weilanden 9, 6708 WG Wageningen, The Netherlands

[§]Department of Chemical and Biomolecular Engineering, Vanderbilt University, Nashville, Tennessee 37235-1604, United States

Supporting Information

ABSTRACT: Capacitive deionization (CDI) as a class of electrochemical desalination has attracted fast-growing research interest in recent years. A significant part of this growing interest is arguably attributable to the premise that CDI is energy efficient and has the potential to outcompete other conventional desalination technologies. In this review, systematic evaluation of literature data reveals that while the absolute energy consumption of CDI is in general low, most existing CDI systems achieve limited energy efficiency from a thermodynamic perspective. We also analyze the causes for the relatively low energy efficiency and discuss factors that may lead to enhanced energy efficiency for CDI.

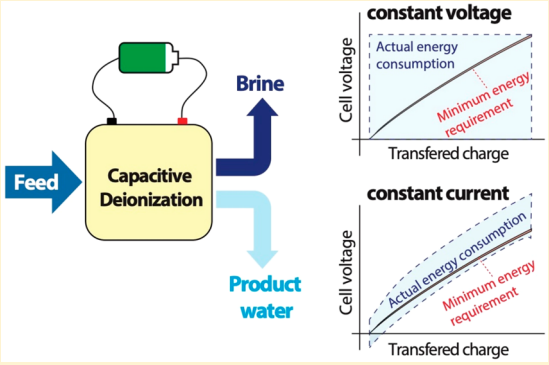

INTRODUCTION

Capacitive deionization (CDI), though it has been invented almost 60 years ago, has started to make significant advances only in the past decade.[1,2] Extensive effort has been devoted to developing high performance electrodes for CDI,[3−13] designing novel cell configurations and operating schemes,[14−24] elucidating fundamental mechanisms of ion adsorption and system behavior,[25−31] and building numerical models that can predict process performance and be used in design optimization.[32−36] A major reason why CDI attracts intensive research interest is the belief that it is an energy efficient desalination technology with a strong potential to compete with the state-of-the-art desalination technologies, such as reverse osmosis (RO), at least for certain applications.[37,38] Indeed, most CDI processes consume less absolute energy to generate a unit volume of product water. However, it is important to realize that the separations achieved by CDI are quite different from those achieved by conventional desalination technologies in terms of the feed salinity and the degree of salinity reduction. Similarly, the separations achieved in different CDI studies are also very different, which poses significant challenges for fair comparison of energy efficiency between different CDI processes.[39,40]

The primary goals of this paper are to survey the literature for assessing the state-of-the-art energy efficiency of CDI and to analyze key factors that influence energy efficiency. In this review, we first describe a framework to assess the energy efficiency of CDI based on comparing the energy consumption of a CDI process with the theoretical minimum energy of the separation achieved by that CDI process. We apply this framework to assess the energy efficiency of CDI processes reported in literature, analyze possible sources of energy losses, and discuss factors that are strongly related to energy efficiency. In addition, we discuss possible reasons that lead to the very high energy efficiency in certain CDI processes with electrodes based on intercalation materials, and provide an empirical correlation using literature data to elucidate the dependence of energy efficiency on several key parameters. The focus of this paper is the energy efficiency of CDI. Other performance metrics are discussed only if they have strong relevance to energy efficiency. For more comprehensive and systematic discussions on various performance metrics and how CDI processes should be holistically evaluated, see several review papers including those by Porada et al.,[41] Suss et al.,[42] and more recently, Hawks et al.[43]

THERMODYNAMICS OF SEPARATION: BENCHMARKING ENERGY CONSUMPTION

As one of the primary considerations in desalination technologies, energy consumption has been widely reported in CDI studies. In all cases, energy consumption is normalized as *specific energy consumption* (*SEC*) that is independent of the system scale.[44] In desalination processes based on salt-rejecting mechanisms, such as RO and thermal distillation, the salinity of the product water is practically zero.[45,46] *SEC* for these processes is usually defined as energy consumed per volume of water produced (example unit: J/L or kWh/m^3). However, the more prevalently used *SEC* in scientific literature of CDI is defined as energy consumed to remove a certain amount of

Received: August 29, 2018
Revised: January 19, 2019
Accepted: February 25, 2019
Published: February 25, 2019

Downloaded via VANDERBILT UNIV on December 29, 2023 at 23:41:38 (UTC).
See https://pubs.acs.org/sharingguidelines for options on how to legitimately share published articles.

ACS Publications © 2019 American Chemical Society

DOI: 10.1021/acs.est.8b04858
Environ. Sci. Technol. 2019, 53, 3366−3378

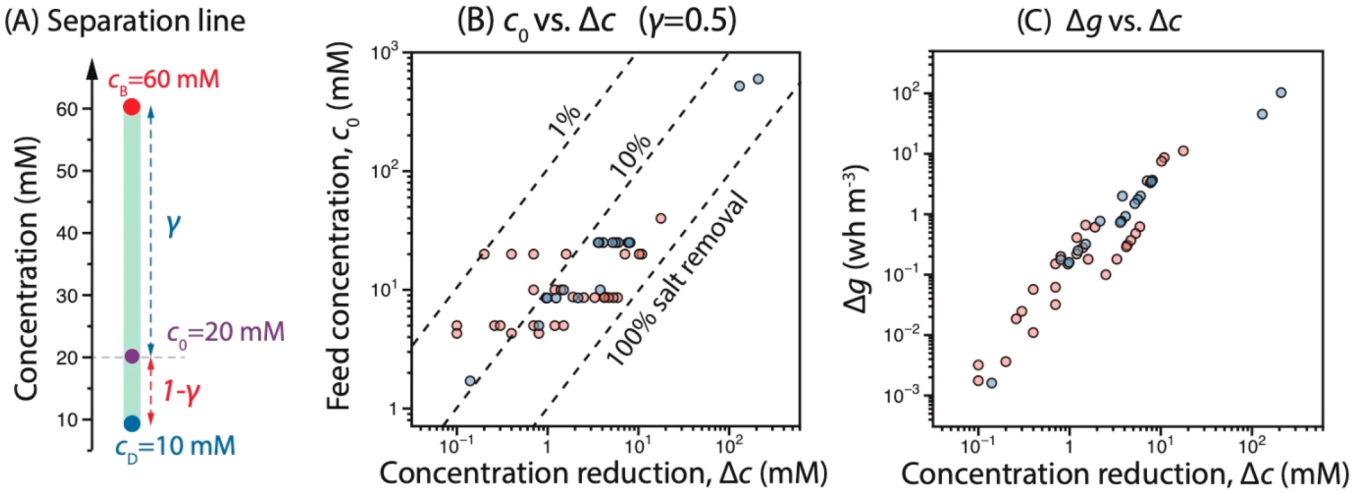

Figure 1. (A) Representative "separation line" that comprises c_0, c_B, and c_D. Water recovery, γ, can be directly determined as the ratio between $c_B - c_0$ and $c_B - c_D$. (B) Summary of the separations using c_0 vs Δc for separations with $\gamma = 50\%$. The dash line represents percentage salinity reduction (e.g., 1%, 10% and 100%). (C) Δg vs Δc for separations presented in panel B. For both panels B and C, red and blue circles represent data points from CDI with carbon electrodes and with electrodes based on intercalation materials, respectively. These data are from Table S1, which will be further analyzed in detail in Figure 2 for energy efficiency.

salts (example units: J/mg, J/mmole, or k_BT/ion),[14,37] mainly because CDI operates based on salt adsorption mechanism and there is a wide spectrum of product water salinity from different studies. Regardless of its definition, *SEC* as an absolute measure of energy consumption cannot be employed to quantify how efficiently energy is spent for achieving a given separation, because some separations are more "difficult" to achieve, and thus intrinsically require more energy, than others. Such "difficulty" of separation can be quantified by the specific Gibbs free energy of separation.[40,47]

A generic separation can be defined by the feed concentration, c_0, the deionized water (i.e., the product water) concentration, c_D, the brine concentration, c_B, and water recovery, γ, defined as the volumetric fraction of the feedwater that is recovered as the deionized water. Three of these parameters are independent according to solute mass balance given by $c_0 = c_B(1 - \gamma) + c_D\gamma$. Graphically, any separation can be visualized using a simple "separation line" (Figure 1A) that contains all the necessary information for defining a separation (see Supporting Information for interpretation of the separation line). An interesting and useful observation is that γ can be directly evaluated from Figure 1A as the ratio between $c_B - c_0$ and $c_B - c_D$. Intuitive comparison between two separations can be performed simply by juxtaposing two separation lines to each other.

For the majority of CDI processes reported in literature, γ is 50%. The separation lines, in this case, are all composed of two equal halves each representing Δc ($= c_0 - c_D = c_B - c_0$). In this case, the representation of separation can further be simplified using a single point on a diagram with c_0 being the *y*-axis and Δc being the *x*-axis (Figure 1B, data from Table S1). Figure 1B suggests that separations achieved in CDI processes reported in literature were dramatically different, with c_0 and Δc both spanning roughly three orders of magnitude. In general, Δc scales with c_0, which is necessary to observe any significant percentage reduction of salinity. However, with a given c_0, Δc can span nearly two orders of magnitude, which suggests that some CDI processes remove a large fraction of salt from the feed whereas some barely remove any. The CDI processes achieving the highest Δc were based on electrodes made of intercalation materials.[48,49]

Thermodynamics of solution suggests that a generic separation defined by c_0, c_D, c_B, and γ always requires a minimum amount of energy to generate a unit volume of product water of concentration c_D.[50] This minimum *SEC*, achievable if and only if the separation is thermodynamically reversible, is the specific Gibbs free energy of separation, Δg,[51,52] which can be obtained by computing the entropy change of the system resulting from the separation:

$$\Delta g = 2RT\left\{\frac{c_0}{\gamma}\ln\left[\frac{c_0 - \gamma c_D}{c_0(1-\gamma)}\right] - c_D\ln\left[\frac{c_0 - \gamma c_D}{c_D(1-\gamma)}\right]\right\} \quad (1)$$

Equation 1 is valid for fully dissociated 1:1 electrolyte solutions. Here, R is the ideal gas constant, and T is the absolute temperature. Like *SEC*, Δg is also normalized by the volume of the product water and is thus independent of the scale of separation. Theoretically, eq 1 is only applicable for ideal solutions. However, the thermodynamic principle that a separation always requires a minimum *SEC* holds also for nonideal solutions. Numerical studies using the Gouy–Chapman–Stern model[52] and the modified Donnan model[51] demonstrate that thermodynamically reversible CDI processes indeed consume Δg. Very recently, Hemmatifar et al. provided an elegant analytical proof that the work consumed by a thermodynamically reversible electrosoprtion process is exactly equal to Δg and that such an equality does not depend on the specific numerical model adopted in describing the EDL as long as parasitic reactions are not considered.[40] Therefore, specific Gibbs free energy sets the baseline for energy consumption of a CDI process. No CDI process, or any desalination process, can consume less *SEC* than Δg. For the data set we analyze, the calculated Δg roughly scale with Δc in a log–log plot (Figure 1C). However, for a given Δc, Δg can vary by more than an order of magnitude depending on other parameters such as feed salinity, which is consistent with eq 1 that shows Δg is not a simple function of Δc.

DOI: 10.1021/acs.est.8b04858
Environ. Sci. Technol. 2019, 53, 3366−3378

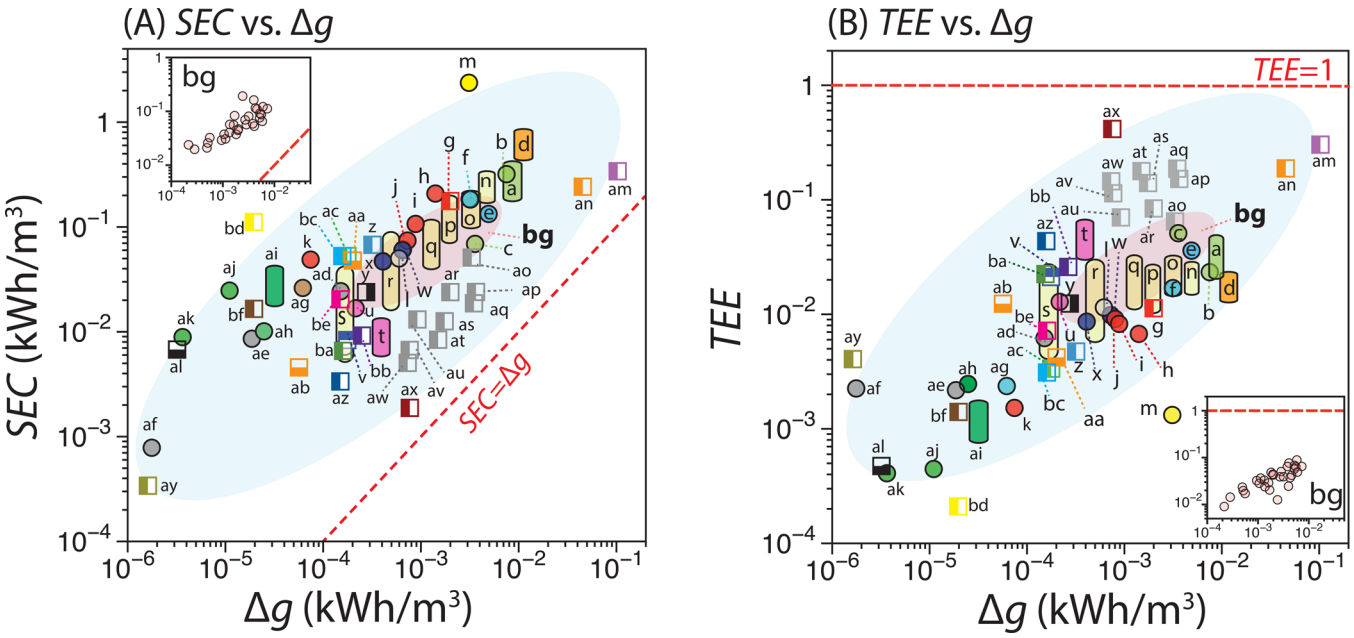

Figure 2. (A) *SEC* as a function of Δ*g*. (B) *TEE* as a function of Δ*g*. The red dash lines are the reference lines representing thermodynamically reversible processes with *SEC* = Δ*g* and *TEE* = 1. Each data point in panels A and B is assigned a letter code with reference listed in Table S1. Different types of symbols represent different types of CDI processes: specifically, the circles refer to CDI with constant voltage (CV) charging and zero voltage (ZV) discharge; bars represent CDI with constant current (CC) charging and reverse current (RC) discharge; squares with solid-left represent CDI with intercalation materials; squares with solid-bottom represent inverted CDI; squares with solid-top ("v") represent CDI with CV charging but non ZV discharge. For CDI and MCDI with CC-RC operation, the bars represent the possible range of *SEC* and *TEE* with controlled RC discharge, depending on the extent (0 to 100%) of energy recovery. Zero energy recovery corresponds to the top of the bars in panel A and bottom of the bars in panel B, while full energy recovery corresponds to the bottom of the bars in panel A and top of the bars in panel B. The "pink ovals" denoted as "bg" in both panels represent the range of data reported in the study of Hemmatifar et al.,[40] with detailed data plotted in the insets. The axes for the insets are the same as those for the main figure.

THERMODYNAMIC ENERGY EFFICIENCY

As Δ*g* quantifies the "difficulty" of the separation a CDI process achieves, it also serves as a reference to evaluate the relative energy efficiency of a CDI process. Such a relative energy efficiency is the thermodynamic energy efficiency (*TEE*), which may allow the direct comparison between CDI processes resulting in different separations. Specifically, *TEE* is defined as the ratio between Δ*g* of a separation and *SEC* of a CDI process resulting in that separation:

$$TEE = \Delta g / SEC \tag{2}$$

TEE represents the fraction of energy spent by a real CDI process that would have been spent by an ideal thermodynamically reversible process achieving the same separation, and can thus quantify the efficiency of energy utilization in a CDI process. By definition, *TEE* ranges from zero to unity. A low *TEE* indicates that only a small fraction of the consumed energy is utilized for separation and a large fraction is dissipated as heat. This concept of *TEE* was employed for systematic performance evaluation by Długołęcki and van der Wal[39] and has been recently revisited systematically by Hemmatifar et al.[40] Here, we use the same approach to analyze a large group of experimental data from CDI studies in literature by first quantifying Δ*g* and *SEC*, and then calculating *TEE* for these reported CDI processes using eq 2. The *SEC* and *TEE* are summarized in Figure 2 (details are reported in Table S1 in the Supporting Information). In most cases, c_0 and γ are directly reported, whereas c_D is the average effluent concentration in the charging step obtained following eq 3:

$$c_D = \frac{1}{\Delta t_c}\int_{t_{c,0}}^{t_{c,f}} c_D(t)\mathrm{d}t \tag{3}$$

where $c_D(t)$ is the effluent concentration at time t during the charging step, $t_{c,0}$ and $t_{c,f}$ are the initial and final time points of the charging step (i.e., $\Delta t_c = t_{c,f} - t_{c,0}$ is the time of charging step). With values for c_0, c_D, and γ, Δ*g* can be calculated from eq 1.

SEC of different CDI processes can be calculated using the following equation if all energy released in the discharge step is recovered:

$$SEC = \frac{1}{v_D}\int_{t_{c,0}}^{t_{d,f}} V_{cell}(t)i(t)\mathrm{d}t \tag{4}$$

where $V_{cell}(t)$ and $i(t)$ are cell voltage and current at time t, and where $t_{d,f}$ is the final time point of the discharge step (i.e., $t_{d,f} - t_{c,0}$ is the full cycle time), and v_D is the volume of the dilute water, which we calculate using $v_D = \phi_D \Delta t_c$ with ϕ_D being the volumetric flow rate of the feed stream in the charging step. Alternatively, one can use $v_D = \phi_D \Delta t_{ads}$, with Δt_{ads} being the period when the effluent concentration is lower than the feedwater concentration, which is, for short desalination cycles, often different from Δt_c. When $V_{cell}(t)i(t)$ is negative, the direction of the current is opposite to that of the cell voltage, and therefore recovery of energy can be achieved by charging an external capacitor or battery. If, however, no energy is recovered during the discharge step, *SEC* is defined as

$$SEC = \frac{1}{v_D}\int_{t_{c,0}}^{t_{c,f}} V_{cell}(t)i(t)\delta_{V,i}\mathrm{d}t \tag{5}$$

DOI: 10.1021/acs.est.8b04858
Environ. Sci. Technol. 2019, 53, 3366−3378

where $\delta_{V,i}$ is a function that yields 1 when $V_{cell}(t)$ and $i(t)$ are of the same direction and 0 when $V_{cell}(t)$ and $i(t)$ are of different directions. In practice, for CDI processes with energy recovery, the efficiency of energy recovery is always less than 100% of the recoverable energy,[53] and consequently, *SEC* falls between the values calculated using eqs 4 and 5. Alternatively, *SEC* is defined based on the amount of salt removed, and therefore the energy consumption is divided by the molar amount, or mass, of salt removed, instead of by ν_D. In this section, we report *SEC* based on the definition of eq 4 (i.e., normalized by ν_D) to be consistent with the reporting method adopted by most other desalination technologies.

To calculate Δg and *SEC* for CDI studies reported in literature, the necessary raw data include the time series of $c_D(t)$, $V_{cell}(t)$, $i(t)$, and values for ϕ_D, Δt_c, and the discharge time, Δt_d. We extracted data from a large number of CDI publications[5,13−15,23,27,37,39,40,48,49,53−70] and analyzed the digitized data to obtain Δg and *SEC* using eqs 1, 3, 4, and 5. For CDI experiments with nonzero voltage discharge (e.g., reverse current discharge), we calculate *SEC* using both eqs 4 and 5 and use those results as the two boundaries of possible *SEC* which represent zero and full energy recovery, respectively. We note that full energy recovery does not mean recovering 100% of the energy spent in the charging step, but rather recovering 100% of the energy released during the discharge step, in which case *SEC* will be calculated by eq 4. These two boundaries define the top and the bottom of the bars in Figure 2A,B representing the possible range of *SEC* and *TEE*. A detailed example regarding the quantification of *TEE* from experimental results is given in the Supporting Information. We note that only papers reporting all necessary information required to calculate *SEC* and Δg were included in the analysis. Therefore, only a fraction of data from the CDI literature (see Table S1) is presented.

Figure 2A,B summarizes the energy efficiency of CDI as *SEC* vs Δg and *TEE* vs Δg, respectively. Comparing these data to the reference lines representing thermodynamically reversible processes, it is clear that most CDI processes reported in literature were thermodynamically highly irreversible. For CDI with carbon electrodes (i.e., not intercalation materials), *SEC* of desalination is typically one to three orders of magnitude higher than Δg of the resulting separation. The highest values of *TEE* seem to be achieved mostly using CDI with intercalation materials,[48,49,64,65] for which we will provide possible explanations in the following sections. The data summarized here follow a similar trend as the data systematically collected in a recent study performed by Hemmatifar et al. (pink "ovals" denoted as "bg" in Figure 2, with details presented in respective insets).[40] In general, CDI processes have a higher *TEE* when they are operated to achieve a more "difficult" separation characterized by a higher Δg (Figure 2B).

The summarized data in Figure 2 show that, though the absolute energy consumption in terms of *SEC* is indeed quite low for most CDI processes (most considerably below 1 kWh m^{-3}), the relative energy efficiency of CDI in terms of *TEE* is quite low due to the very low Δg typical of separations achieved by CDI. Most CDI processes based on carbon electrodes did not achieve a *TEE* above 10%. Nevertheless, *TEE* above 10% was achieved in four recent CDI studies using intercalation materials as electrodes,[48,49,64] with the highest reaching 40%,[65] which is in the same order of magnitude as RO, the state-of-the-art desalination technology (a summary of *TEE* for RO applied to both seawater and brackish water desalination is listed in Table S3, and a recent simplified theoretical comparison of energy consumption between CDI and RO is given by Qin et al.).[71]

■ SOURCES OF ENERGY LOSSES IN CDI, AND WHY CAN *TEE* BE VERY LOW?

How can one explain the generally very low values for *TEE* reported for CDI? The first important reason is that most data in Figure 2 were acquired in CDI experiments using zero voltage (ZV) discharge with which no energy is recovered. With carbon electrodes, a large fraction of the energy spent in the charging step is stored in the electrical double layers (EDLs). Recovering this energy stored in the EDLs during the discharge step can enhance *TEE*.[39,72] When the energy stored in EDLs is completely recovered, the values of *TEE* can be increased from the bottom to the top of the bars plotted in Figure 2B. We note that neither the energy consumed in the charging step nor the energy stored in the EDLs can be fully recovered. The theoretically recoverable energy is the energy consumed in the charging step minus the resistive energy losses in both the charging and discharge steps. In practice, a significant fraction of this theoretically recoverable energy can be recovered by a buck-boost converter in the discharge step.[53,73]

Using flow-by CDI and MCDI (i.e., CDI with ion exchange membranes) processes with constant current charging and reverse current discharge (i.e., CC-RC operation) as examples, we illustrate the different contributions to the energy loss in Figure 3. We assume a current density of 30 A/m^2 and the absence of Faradaic energy loss in our numerical simulation using a one-dimensional dynamic steady-state model. The separation achieved is characterized by c_0 = 20 mM (1:1 electrolyte), c_D = 12 mM, and γ = 50% (thus c_B = 28 mM). Different voltages and potential drops are plotted in Figures 3A (for CDI) and 3B (for MCDI) as a function of electrode charge density, σ, which quantifies to what extent the CDI cell has been charged or discharged. In Figure 3A and 3B, the dashed curves represent the potential drop over the EDL (Stern and Donnan). The thickness of each color-coded region represents the potential drop due to one of several resistances (to be elaborated) or due to the difference of the Donnan potentials at both ion exchange membrane (IEM) interfaces. The models used to generate all panels in Figure 3 have been reported in detail in the literature[35] and are summarized in the Supporting Information.

In the case of CDI without IEM, three major categories of energy losses are considered.[74−76] The first category arises from the electronic resistance in the solid matrix of the electrodes, current collectors, connecting wires, and the imperfect contacts between these components. The second category stems from the ionic resistance in the macropores arising from the limited rate of ion transport through the macropores. The third category is associated with the ionic resistance of the spacer channel due to the limited rate of ion transport across the spacer channel to enter the macropores. The corresponding potential drops of these three categories, denoted as ΔV_e, $\Delta V_{i,mA}$, and $\Delta V_{i,sp}$, are represented by the thicknesses of the red, blue, and yellow regions, respectively. We note that the relative importantance of these contributions is system dependent.

The dashed curve in Figure 3A represents the sum of the Donnan and Stern potentials, or in other words, the equilibrium voltage, V_{eq}.[35] As a function of σ, $V_{eq}(\sigma)$ can be

DOI: 10.1021/acs.est.8b04858
Environ. Sci. Technol. 2019, 53, 3366−3378

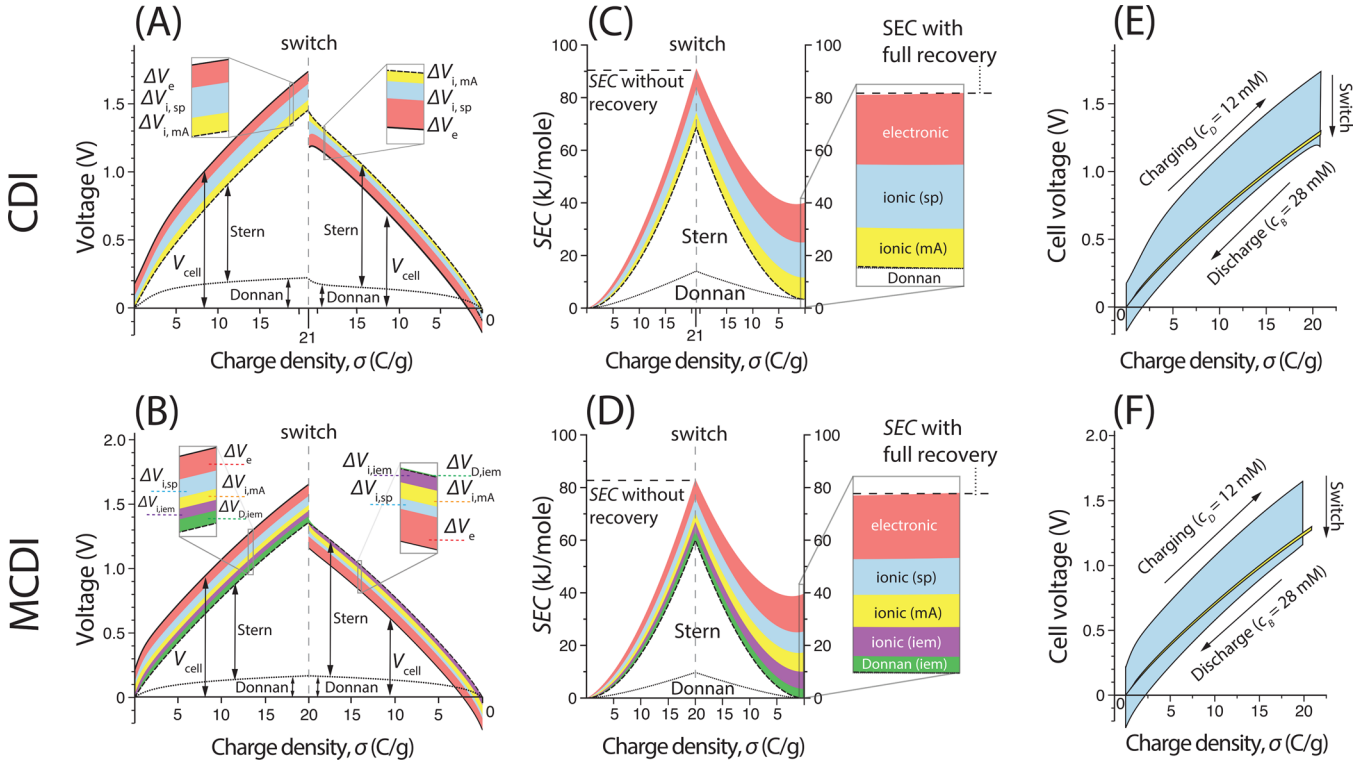

Figure 3. (A and B) Different voltages and potential drops as functions of charge density, σ, for CDI and MCDI processes with CC-RC operations, respectively. The solid curves and dash curves represent V_{cell} and V_{eq} (i.e., the sum of Stern and Donnan potentials). The thickness of each color-coded region represents a potential drop due to the electronic resistance (red), the ionic resistance in the macropores (yellow) or in the spacer channel (blue) in both CDI and MCDI. For MCDI, the potential drop due to the ionic resistance in the IEMs (purple) and due to the difference between the Donnan potentials at both membrane interfaces (green) are also plotted. (C and D) Cumulative *SEC* and its contributions from different mechanisms as a function of σ for CDI (panel C) and MCDI (panel D), respectively. The color code for different mechanisms is identical to that used in panels A and B. (E and F) Simulated cycles with flow-by CC-RC operations (contours of blue region, including the yellow region) and the corresponding thermodynamically reversible cycles (contours of the very thin yellow regions) resulting in the same separation, for CDI (panel E) and MCDI (panel F), respectively. The areas of blue and yellow regions are proportional to *SEC* (with complete energy recovery) and Δg, respectively. In panels A to D, the vertical dash line marked as "switch" represents the end of the charging step when the current direction is switched. The detailed equations and parameters used to generate all the curves in this figure are presented in the Supporting Information.

interpreted as the cell voltage required to maintain the existing σ and ion distribution without either discharging or further charging the system. If a CDI cell is always charged at a cell voltage that is infinitesimally higher than V_{eq}, the current density will be infinitesimal and there is no resistive energy loss. Obviously, this is not a practical operation condition as desalination will take infinitely long.

The total potential drop due to ionic and electronic resistances, quantified by the total thickness of the color-coded region in Figure 3A, is the difference between V_{cell} and V_{eq}. This total potential drop is the excess voltage, V_{ex}, required to operate the CDI system at a certain current density. The positive value for V_{ex} in the charging step suggests that energy is dissipated to charge the cell at a certain current density, and the negative V_{ex} in the discharge step implies that energy is also dissipated to discharge the cell (i.e., not all capacitive energy is recoverable). We note that V_{ex} does not increase with current density linearly, because the ionic resistance depends on the spacer channel salinity, which in turn on depends on current density.

Similar charging and discharge curves are also simulated for MCDI to achieve the same separation at the same current density (Figure 3B). Similar to the description of CDI in Figure 3A, the same concepts of V_{eq} and V_{ex} can be defined for MCDI. Compared to CDI without IEM, two extra potential drops are present in MCDI, including (i) the drop arising from the ionic resistance in the IEM, $\Delta V_{i,mem}$, and (ii) the sum of the Donnan potentials at the two interfaces of the IEMs, $\Delta V_{D,mem}$. The V_{eq} for MCDI includes $\Delta V_{D,mem}$ which originates from ion distribution instead of ion movement, whereas $\Delta V_{i,mem}$ adds to V_{ex} and contributes to the resistive energy losses. We note that σ at the end of the charging step is higher for CDI (batch cycle, reversible) than for an MCDI process achieving the same separation, because MCDI, with a higher charge efficiency, transfers less charge than CDI to remove the same amount of salt.

Another informative way to present the breakdown of energy consumption in CDI and MCDI processes is to plot cumulative specific energy consumptions as a function of σ for the full charging/discharge cycle (Figure 3C,D), similar to what has been shown by Dykstra et al.[76,77] Surprisingly, even though the charge efficiency of MCDI is higher than that of CDI, *SEC* of the two processes, both achieving the same separation and with the same current density, are very similar (without considering possible Faradaic reactions). This may be explained by the fact that the additional $\Delta V_{D,mem}$ and $\Delta V_{i,mem}$ in MCDI is offset by the significant reduction of $\Delta V_{i,mA}$ due to the much higher macropore concentration enabled by the IEMs.

DOI: 10.1021/acs.est.8b04858
Environ. Sci. Technol. 2019, 53, 3366−3378

The definition of *SEC* based on eq 4 suggests that *SEC* is simply proportional to the area of the cycle encompassing the blue and yellow regions in Figure 3E, if complete energy recovery is assumed. Such a cycle is obtained by horizontally flipping the solid discharge curve (i.e., V_{cell} vs σ) about the axis denoted as "switch" in Figure 3A. In comparison, Δg is proportional to the area of the very thin yellow cycle in Figure 3E. The yellow cycle represents a thermodynamically reversible CDI cycle obtained using a batch CDI operation. In this specific illustrative example, *SEC* and Δg are 110 and 4.5 Wh/m^3, respectively, which leads to a *TEE* of 4.07%. Similar comparison between *SEC* and Δg can also be performed using Figure 3F for MCDI, which results in a *TEE* of 4.11%.

The analyzed example, characterized with a *TEE* of only ~4.1%, reveals a very important insight for understanding the energy efficiency of CDI or MCDI. In the field of supercapacitors, which are energy storage devices based on the same fundamental principle as CDI, a common metric is the efficiency of energy storage (or "round-trip" efficiency), which is defined as the ratio between the energy released in the discharge step and the energy spent in the charging step.[38,78] Applying the same concept in CDI, Figure 3E,F suggests that over 50% of energy consumed in the charging step can be theoretically recovered in the discharge step, even if we consider all the resistive energy losses. However, *TEE* by the definition based on eq 2 has been calculated to be only 4.1%. It is of paramount importance to realize that the definitions of "round-trip" efficiency in supercapacitor energy storage and the energy efficiency in CDI are fundamentally different, which can be illustrated using Figure 3E,F. The efficiency of energy storage, if the system were treated as a supercapacitor, is equal to the ratio of the area below the discharge curve (but above $V_{cell} = 0$) and the area below the charging curve plus the area of the small "triangle" below $V_{cell} = 0$, which is reasonably large.[79] *TEE*, however, is quantified by the ratio between the area of the yellow region, which is very small, and that of the blue region (including the yellow region). Such graphical illustrations clearly show why *TEE* is typically significantly lower than the "round-trip" efficiency of energy storage if the CDI system were treated as a supercapacitor.

In addition to CDI with CC-RC operation, another example that is more often encountered yet easier to analyze for energy efficiency is CDI with constant voltage charging and zero voltage discharge (CV-ZV). Figure 4 shows a CV-ZV cycle in which the CDI cell is charged and discharged to equilibrium (i.e., $V_{ex} = 0$ at the end of charging and discharge steps). The separation resulting from this CDI cycle is chosen to be exactly the same as that achieved in the CDI and MCDI process shown in Figure 3. Such a CDI cycle with CV-ZV operation is represented in the "V_{cell} vs σ" diagram as a rectangle with its height representing the charging voltage. For the specific case shown in Figure 4, *SEC* and Δg are 303.8 and 4.5 Wh/m^3, respectively, which results in a *TEE* of 1.5%.

Unlike CDI with CC-RC operation in which the energy consumed for transferring a unit charge is strongly dependent on current density and cell resistance, the energy consumption per transferred charge in CV charging is always eV_{cell} (e is the elementary charge). In addition, V_{ex}, as a function of σ, is independent of cell resistance as long as the target separation is achieved by charging and discharging the system to equilibrium (Figure 4). With CC-RC operation, as the desalination rate is roughly proportional to current density and is thus constant, the resistive energy loss strongly depends

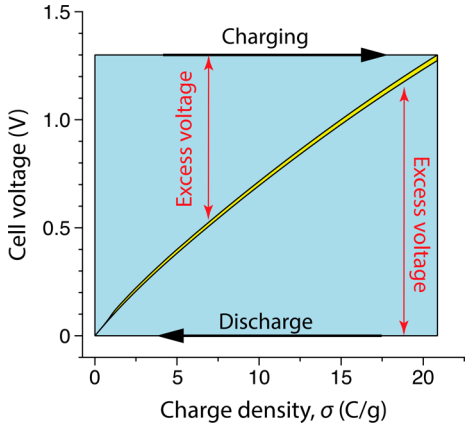

Figure 4. CV-ZV cycle, as represented by the contour of the blue rectangle (including the yellow region), and the corresponding thermodynamically reversible cycle resulting in the same separation, as represented by the contour of the thin yellow region. The resulting separation is the same as that in Figure 3E,F.

on cell resistances. With CV-ZV operation, however, the resistive energy loss is proportional to the area of the blue region (excluding the yellow region) in Figure 4 and is thus independent of cell resistance. Therefore, for CDI that is operated in a CV-ZV mode and charged/discharged until equilibrium is reached, *TEE* is already determined once the cell voltage is specified, if parasitic energy losses due to leakage current and Faradaic reactions are not considered. It is important to emphasize again that Figure 4 only applies to CV-ZV operations in which equilibrium is reached at the end of the charging step. This may require prolonged charging as the driving force for charge transfer vanishes at the end of the charging step. Faster charging can be achieved by applying a V_{cell} higher than the V_{eq} at the end of the charging step to sustain a positive driving force (i.e., V_{ex}) throughout the charging step, in which case more energy will be consumed for the same separation and *TEE* will decrease accordingly.

Last but not least, there is one additional and important energy loss mechanism that is difficult to accurately simulate using the "V_{cell} vs σ" diagrams shown in Figures 3 and 4. The parasitic Faradaic reactions that transfer charge to sustain reduction/oxidation reactions at the water/electrode interfaces can result in additional charge transfer that does not contribute to ion removal.[80] This effect is actually considered in charge efficiency, an important metric to be discussed later. Graphically, this makes the blue boxes in Figures 3E,F and 4 considerably longer (in the direction of x-axis) than the yellow reversible cycle that they encompass, which in turn leads to significantly lower *TEE*. For this reason, MCDI, especially at high current density, is more efficient than CDI without IEMs not only because IEMs mitigate co-ion repulsion from the electrode regime, but also because the presence of IEMs mitigates Faradaic reactions.[81]

■ HIGH *TEE* IN (SOME) CDI PROCESSES WITH INTERCALATION MATERIALS

The pursuit of intercalation materials as promising CDI electrode material has been primarily driven by the belief that they can yield much higher specific adsorption capacity (*SAC*) as compared to conventional carbon-based electrodes.[9,82−86] The higher *SAC* is attributable to the ability of intercalation materials to store ions in their solid phase (i.e., the crystal

DOI: 10.1021/acs.est.8b04858
Environ. Sci. Technol. 2019, 53, 3366−3378

structure),[85,87] as compared to carbon electrodes that store ions by forming EDLs in the micropores. Interestingly, the summary of *TEE* in Figure 2 suggests that some CDI processes using electrodes based on intercalation materials (i.e., im-CDI, with "im" representing intercalation materials) also achieved significantly higher *TEE* than CDI with carbon electrodes. In fact, according to the studies covered in Figure 2, values of *TEE* higher than 10% were only achieved using im-CDI.

In theory, intercalation materials do not seem to have significant direct advantage over carbonaceous materials in terms of reducing cell resistance and resistive energy loss. In fact, most intercalation materials have poor electronic conductivity,[88,89] which is detrimental to achieving high energy efficiency. However, intercalation materials have two major advantages that allow im-CDI systems to be operated in ways that significantly benefit *TEE*. The first advantage is the high *SAC*. Even though *SAC* is not directly relevant to *TEE*, the high *SAC* of intercalation materials enables im-CDI to remove a considerable amount of salt and thereby achieve an appreciable percentage reduction of salinity even when it is employed to desalinate high salinity feed solution.

This advantage has two implications. First, increasing the salinity reduction increases Δg, which has a very strong positive impact on *TEE* according to eq 2. This has been clearly demonstrated by the positive correlation between *TEE* and Δg shown in Figure 2B. In other words, the higher *SAC* of im-CDI allows it to achieve more "difficult" separations that are strongly beneficial to achieving higher *TEE*. Second, as im-CDI can be employed to desalinate high salinity feed solution, the higher feed salinity, c_0, reduces the ionic resistances in the spacer channel and the macropores which together comprise a significant portion of the overall resistance. The reduced resistance may have a significant impact on *TEE* if the im-CDI system is operated in a CC-RC mode. However, most im-CDI studies were performed using CV-ZV mode, in which case the impact of cell resistance is primarily on desalination rate.

The second advantage of intercalation materials is the lower V_{cell} than that of carbon electrodes for achieving significant salt removal.[48,49,70] This is attributable not only to the higher *SAC* of intercalation materials, but also to the working mechanism of electrodes based on intercalation materials.[85,87] In the case of carbon electrodes with which salt removal is based on the formation of EDLs, V_{eq} rises very sharply as the electrodes are charged. A significant part of V_{eq} is the Stern potential as shown in Figure 3A,B. Electrodes with intercalation materials employ very different mechanisms for ion storage, with which the equilibrium may be described by the Frumkin intercalation isotherm.[87,90,91] For electrodes based on intercalation materials, the increase of V_{eq} as a function of charge density is significantly slower than that for carbon electrodes. In other words, im-CDI stores less energy in the charging step than CDI based on carbon electrodes for removing the same amount of salt.

With CC-RC operation, the amount of "stored energy" at the end of the charging step theoretically does not have impact on energy consumption if it can be fully recovered (excluding the resistive loss) in the discharge step, as in this case the energy consumption is primarily the resistive energy loss. However, no practical CDI process can fully recover the "stored energy" in the discharge step, which renders im-CDI more advantageous as less "stored energy" is available to lose. This is even more the case for CV-ZV operation adopted by most reported studies evaluated in this paper, as all "stored energy" is lost with ZV discharge. As Figures 3E,F and 4 illustrate, *TEE* is simply the ratio between the area of the yellow cycle (representing Δg) and the area of the blue boxes (representing *SEC*). The use of im-CDI, which has a lower V_{eq} at a given charge density, lowers the height and reduces the size of the blue rectangle, and thereby leads to a higher *TEE*.

Based on the definition of *TEE* and following the above analysis, there should be a correlation between *TEE*, Δg, Δc, Λ_{dyn} and ΔV_{cell}, following the form described in eq 6

$$TEE \approx \beta \frac{\Delta g \Lambda_{dyn}}{\Delta V_{cell} \Delta c} \tag{6}$$

Here, ΔV_{cell} is the difference between the charge-averaged (i.e., not time-averaged) voltages in charging and discharge steps, which is exactly equal to the charging voltage for CV-ZV operation and roughly equal to the average height of the blue region in Figure 3E,F for CC-RC operation, and Λ_{dyn} is the dynamic charge efficiency to be further discussed in the section after next. The coefficient β is a constant that depends on the specific units chosen for the parameters. Equation 6 is proposed based on the argument that SEC_w is roughly proportional to $\Delta V_{cell}\Delta c/\Lambda_{dyn}$ (Supporting Information for detailed explanation).

We apply eq 6 to a subset of the data in Table S1 that provide sufficient information to calculate ΔV_{cell} and Λ_{dyn}. The results suggest that the correlation given by eq 6 works reasonably well, especially for im-CDI (Figure 5). The goodness of fit is less satisfactory for CDI with carbon electrodes, but the overall trend of *TEE* is successfully captured by the correlation. This correlation can be employed to justify the very high *TEE* of some im-CDI processes. For example, the two data points with the highest *TEE* were obtained from an im-CDI study that used a V_{cell} of only 0.55 V and ΔV_{cell} as low as 0.1 V,[48,49] considerably lower than that in most other studies, to achieve values of Δg that are one to several orders of magnitude higher than that achieved by other studies.

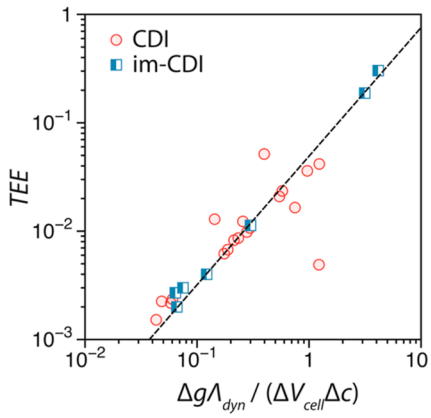

Figure 5. *TEE* vs $\Delta g\Lambda_{dyn}/(\Delta V_{cell}\Delta c)$ for CDI with carbon electrodes (red circles) and im-CDI with electrodes based on intercalation materials (blue squares). The coefficient of determination is R^2 = 0.82. The specific position of the data cluster is dependent on the choice of units for different parameters, but the relative positions of the data points in the cluster and the goodness of fit is independent of unit choice.

Lastly, it is important to point out that many im-CDI systems employ a configuration that is fundamentally different from most configurations used in CDI with carbon electrodes.

DOI: 10.1021/acs.est.8b04858
Environ. Sci. Technol. 2019, 53, 3366−3378

While a silver electrode has been used as anion (Cl^-) electrode in one im-CDI study,[49] other im-CDI studies adopt a configuration that involves two cation intercalation electrodes (i.e., no electrode for anion adsorption) separated by an odd number of IEMs.[64,70,84,85] The working mechanism of im-CDI systems with such a configuration is to a great extent similar to electrodialysis. Due to the very different configurations and ion-removal mechanisms between this specific type of im-CDI and typical CDI, the results from the above analysis comparing the energy efficiency of im-CDI and CDI must be interpreted with caution.

ENERGY EFFICIENCY AND DESALINATION RATE: AN INTRINSIC TRADE-OFF OF SIGNIFICANCE

In this section, we will discuss how the desalination rate affects *TEE*, as desalination rate is strongly related to ΔV_{cell}, which has a strong impact on *TEE* according to eq 6. In general, an effective way to enhance *TEE* is to reduce the resistive energy loss, which is graphically equivalent to reducing the area of the blue regions in Figures 3E,F and 4. With CV-ZV operation, this can be achieved by reducing the charging voltage. However, a reduced charging voltage leads to a reduced excess voltage which, with the same cell resistance, inevitably results in slower desalination. This inherent trade-off between energy efficiency and desalination rate can also be quantified using the example of CC-RC operation in which desalination rate is roughly proportional to the current density that is constant. Here, we will quantify such a trade-off by systematically evaluating an MCDI process with CC-RC operation at different desalination rate.

The quantification of desalination rate and energy consumption typically requires normalization to obtain scale-independent performance metrics. There are two general approaches for normalization. In the first approach, the performance metrics are normalized by the amount of removed salt. In this case, the desalination rate is quantified using average salt adsorption rate (*ASAR*), defined as the amount (either mass or mole) of salt adsorbed by unit electrode mass in unit time,[42] and *SEC* is defined as energy consumed per amount (either mass or mole) of salt removed (example unit: J mol^{-1}).[44] We denote *SEC* with this definition as SEC_i with the subscript "i" representing "ions".

The second approach, which is more relevant for practical evaluation and optimization of CDI processes for which Δc has been specified as the treatment goal, involves normalizing the desalination rate by the volume of the deionized product water. With this approach, the desalination rate is quantified by productivity, *P*, defined as the volume of product water generated by a unit area of electrode in a unit time.[43] Productivity has exactly the same unit as flux that is extensively used to quantify the desalination rate in RO. *SEC* in this case is defined as energy consumed to produce a unit volume of deionized water (example unit: Wh m^{-3}), which we will denote as SEC_w with the subscript "w" representing "water". SEC_w is also consistent with the adopted approach for quantifying energy consumption in RO.[92,93] We note that the approach of normalizing by the amount of removed salt is the most adopted approach for reporting *SEC* in most existing CDI literature, because SEC_i is more sensible than SEC_w for comparing different CDI processes with different salinity reduction.

A trade-off curve can be constructed by plotting either the inverse of SEC_i (i.e., SEC_i^{-1}) as a function of *ASAR* or the inverse of SEC_w (i.e., SEC_w^{-1}) as a function of *P*. We note that SEC_i^{-1} has the same meaning as energy normalized adsorbed salt, *ENAS*.[75] The use of the inverse of *SEC* instead of *SEC* itself leads to a trade-off curve that is monotonically decreasing, which is a more intuitive representation of a trade-off relationship. We note that the conversion between SEC_i (or *ENAS*) and SEC_w, and between *ASAR* and *P*, can be readily performed if the salinity reduction Δc (= $c_0 - c_D$) and flow rate are known.[43,94] A trade-off curve is meaningful only if all points on a trade-off correspond to the same separation. While current density can be readily controlled, the key in establishing a trade-off curve in flow-by CDI processes is to simultaneously adjust the feed flow rate so that Δc remains constant at different current densities. Using this approach, trade-off curves have been established both experimentally and by simulation.[43,94] For illustration, simulated trade-off curves are presented in Figure 6.

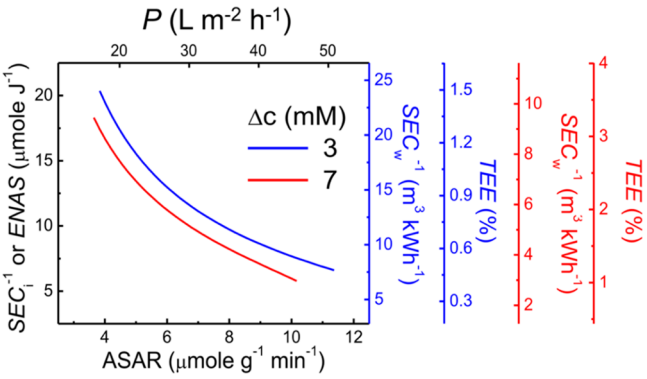

Figure 6. Example trade-off curves that quantify the relationship between desalination rate (*ASAR* or *P*) and energy efficiency (*ENAS*, SEC_w^{-1}, or *TEE*). The trade-off curves are simulated for an MCDI process with a feed solution of 20 mM and a water recovery of 50%.

The trade-off curves in Figure 6 suggest that energy efficiency, as quantified by either inverse of *SEC*, is roughly inversely proportional to desalination rate, as quantified by either *ASAR* or *P*. Because all points on a trade-off curve correspond to the same separation and thus the same Δg, *TEE* is simply proportional to SEC_w^{-1} for a given trade-off curve (Figure 6, additional *y*-axis). Therefore, *TEE* is also inversely proportional to desalination rate. Because each trade-off curve illustrated in Figure 6 involves a single MCDI system and results in the same separation, it suggests that *TEE* does not only depend on the resulting separation or the "goodness" of the CDI system but also strongly on how fast the CDI process is performed to achieve the target separation. Enhancing the desalination rate inevitably consumes more energy (moving down the trade-off curve), and vice versa.

CHARGE EFFICIENCY: CORRELATION TO ENERGY CONSUMPTION REVISITED

Another important and widely investigated performance metric strongly related to energy efficiency is the charge efficiency, Λ.[95−98] Charge efficiency, defined as the amount of adsorbed salt over transferred charge, quantifies how efficient a CDI process utilizes charge transfer for ion adsorption.[41,61] A recent study by Hawks et al. suggests that the charge efficiency calculated using experimentally measured effluent salinity, which has been named dynamic charge efficiency, Λ_{dyn}, is not

DOI: 10.1021/acs.est.8b04858
Environ. Sci. Technol. 2019, 53, 3366−3378

exactly Λ by its very definition.[99] The discrepancy is attributable to the fact that the charging step actually removes more salt from the feed solution than the measured salinity reduction suggests, as some adsorbed salt is released back to the deionized solution (in the spacer channel) that has not exited the CDI cell upon the charging/discharge switch. A metric named flow efficiency, Λ_{flow} (= Λ_{dyn}/Λ), which was introduced by Johnson and Newman,[100] was adopted to account for this effect. The flow efficiency is close to unity, which is desirable, if the residence time is considerably shorter than the charging time. We note that Λ_{flow} cannot be directly measured using experiments but has to be evaluated using a model with certain assumptions.[99] In addition to the effect accounted for by Λ_{flow}, we note that Faradaic reactions also contribute to reduced charge efficiency.

Many studies have been performed to investigate the dependence of Λ_{dyn} on operating conditions.[14,27,32,61] It has been suggested, with supporting experimental evidence, that *SEC* negatively correlates with Λ_{dyn}.[42] Specifically, an inverse proportionality has been proposed to capture the dependence of SEC_i on Λ_{dyn} (see Figure 5 in the classic review paper by Suss et al.).[42] Such a conclusion was primarily based on one large experimental data set in which the SEC_i and Λ_{dyn} were measured at different influent feed salinities with or without IEMs.[14] The most salient feature is that SEC_i has a clear negative correlation with Λ_{dyn}, which is particularly strong when Λ_{dyn} is low.

The inverse proportional correlation between SEC_i and Λ_{dyn} is theoretically justified by simply combining eqs 2 and 6 and noting that $SEC_i = SEC_w/\Delta c$:

$$SEC_i = \frac{1}{\beta}\frac{\Delta V_{cell}}{\Lambda_{dyn}} \tag{7}$$

However, eq 7 also suggests that SEC_i is strongly dependent on ΔV_{cell}. This implies that any inverse proportionality observed in a series of data is not universal but rather conditional upon the requirement of constant ΔV_{cell} for all data points in that series (e.g., all data points in such a series were collected from CV-ZV operation with the same charging voltage). That is, SEC_i is not a simple one-to-one function of Λ_{dyn} as a universal inverse proportionality would have suggested.

For example, we analyze a set of data obtained in a recent study of MCDI with CC-RC operation and different operating conditions.[94] Because of the presence of IEMs, Λ_{dyn} is relatively high for the entire data set. The correlation between SEC_i and Λ_{dyn} is very weak (Figure 7A): within a relatively small range of relatively high values for Λ_{dyn} (from 0.70 to 0.97), SEC_i varies, without observable trend, from 0.054 to 0.243 J/μmol. Specifically, comparing data from experiments performed with two different sets of electrode materials suggests that the FM10K carbon cloth electrodes (red circles in Figure 7) consume more energy than PACMM electrodes (blue circles in Figure 7A) for achieving the same separation, even when their Λ_{dyn} values are very similar. Performing the same analysis using Λ, which was calculated using Λ_{dyn} and the flow efficiencies estimated using the approach proposed in ref 99, slightly shifts the position of the data cluster but did not change the qualitative conclusion of the lack of correlation.

Dynamic charge efficiency is of critical significance because a low Λ_{dyn} means a large fraction of the energy is spent on charge transfer that does not result in ion removal from the bulk solution.[42,61,95] The "wasted" charge transfer can be attributed to co-ion repulsion, unintended discharging into already deionized water (as characterized by flow efficiency), and in some cases, also to Faradaic reactions. In contrast, a high Λ_{dyn} means that most of the energy is spent on charge transfer that results in ion removal from the bulk solution. Therefore, Λ_{dyn} quantifies the "utility" of charge transfer. However, SEC_i does not only depend on the utility of charge transfer but also strongly depends on how much energy is actually consumed to transfer charge, which is roughly quantified by $e\Delta V_{cell}$. Therefore, while a CDI process with low Λ_{dyn} cannot be energy efficient, a CDI process with very high Λ_{dyn} is not necessary energy efficient as much energy can be consumed for charge transfer (e.g., when resistance is high and/or desalination rate is fast, which leads to a large ΔV_{cell}). In summary, a high Λ_{dyn} is only a necessary, but not a sufficient, condition for an energy-efficient CDI process.

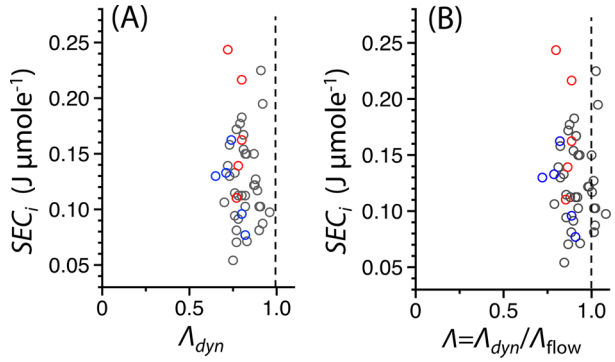

Figure 7. (A) *SEC* vs Λ_{dyn} and (B) *SEC* vs Λ (= $\Lambda_{dyn}/\Lambda_{flow}$) for a series of data obtained using MCDI experiments reported in ref 94. We note that $\Lambda > 1$ is observed, likely due to errors in estimating the flow efficiency using a model with several ideal assumptions and/or the uncertainty in estimate the cell's fluid volume.

■ PERSPECTIVES, LIMITATIONS AND SIGNIFICANCE

The recent intensive research pursuit in CDI has been to a certain extent motivated by the promise that CDI may soon become a low-energy-consumption alternative to conventional and more mature desalination technologies. On the one hand, CDI is indeed a low-energy-consumption technology, as the majority of CDI studies have reported SEC_w values that are significantly lower than that of any typical desalination technology. On the other hand, the very low SEC_w values of many CDI processes do not suggest that they are highly energy efficient, because the majority of reported CDI processes were employed to achieve "easy" separations that intrinsically require very little energy. The concept of *TEE* helps us account for the "difficulty" of separation when interpreting the energy consumption and assessing the energy efficiency of CDI processes. While no study on CDI with carbon electrodes has yet shown a *TEE* higher than 10%, CDI with electrodes based on intercalation materials have shown values of *TEE* as high as 40%. These results suggest that it is possible for CDI to achieve a *TEE* in the same order of magnitude as that for RO, the state-of-the-art desalination technology. Our analysis also suggests that several factors are associated with a high *TEE*. These factors, which are summarized in Table 1, contribute to either a higher Δg or a lower *SEC*.

It is important to emphasize that, although *TEE* is an important performance metric, it is not a very useful

DOI: 10.1021/acs.est.8b04858
Environ. Sci. Technol. 2019, 53, 3366−3378

Table 1. Summary of Factors Associated with High *TEE*

	Factors	Mechanism	Note
A	high salinity feed solution[a]	• reduce ionic resistance (*SEC* ↓)	Reduced ionic resistance increases *TEE* for CC-RC operation. For CV-ZV, it leads to faster desalination and does not affect *TEE*.
B	more salinity reduction[a]	• more difficult separation (Δg ↑)	
C	energy recovery in the discharge step	• reduce effective energy use (*SEC* ↓)	Must be implemented to achieve very high *TEE*.
D	improved electrode and cell design	• reduce electronic and/or ionic resistance (*SEC* ↓) • minimize parasitic loss (*SEC* ↓) • improve flow efficiency (*SEC* ↓)	The most recognized strategy to enhance CDI performance. For CV-ZV, it leads to faster desalination and does not affect *TEE*.
E	low desalination rate[b]	• reduce "driving force" (*SEC* ↓)	Can be achieved by charging at low current density or voltage[c]. Loss due to parasitic reactions become significant when desalination rate is too low.[40]
F	high charge efficiency Λ_{dyn}	• maximize the "utility" of charge transfer (*SEC* ↓)	Λ_{dyn} should be maximized but high Λ cannot guarantee high *TEE*.
H	use of intercalation materials as electrodes	• more salinity reduction (see B, Δg ↑) • reduce charging voltage for the same separation (*SEC* ↓)	Lower charging is particularly benefitial to *TEE* when energy recovery is poor or absent.
I	batch mode	• eliminate "flow system limitations"[d] (*SEC* ↓)	Relatively insignificant impact on practical systems unless *TEE* becomes very high.

[a]For a given desalination need (i.e., reducing the feed salinity to a target effluent salinity), these are not practical strategies to reduce energy consumption. [b]Lower desalination rate leads to a larger system and higher capital costs. [c]If the system is charged in CV mode until equilibrium is reached, charging voltage depends on the equilibrium charge density required by the target separation and cannot be freely adjusted. In other words, V_{cell} can be adjusted in CV mode to achieve the same separation but different desalination rate only if V_{cell} is higher than V_{eq} at the end of the charging step. [d]See Supporting Information for further explanation of "flow system limitations."

performance metric for the purpose of designing and optimizing a CDI system to meet a certain desalination requirement (i.e., reducing the feed salinity to a target effluent salinity). While we understand that achieving higher Δg is beneficial to enhancing *TEE*, we cannot and should not desalinate more saline feedwater just for pursuing a higher *TEE*. Even with a given feed solution, we should not desalinate more than necessary to achieve a higher Δc just for a higher *TEE*, as doing so will lead to higher SEC_w which has more direct relevance to cost of water production. In general, it has been proposed that the technoeconomic analysis of CDI systems should simultaneously consider energy efficiency and desalination rate on the basis of their trade-off relationship.[43,94] In this context, the energy consumption should be quantified using SEC_w which is more relevant (than *TEE*) to practical cost consideration.

The use of *TEE* as a performance metric, however, helps us acquire a better understanding of how efficient various CDI processes are, which cannot be judged based on absolute performance metric such as SEC_i or SEC_w. For a specific CDI process, *TEE* helps us gauge how much room there is to further enhance the energy efficiency and understand the limit of *SEC* (which is essentially Δg). Within the CDI research field, *TEE* enables us to compare across different processes that result in different separations and to identify strategies for enhancing the energy efficiency of CDI. Last but not least, *TEE* is the only performance metric that allows direct comparison of energy efficiency between different desalination technologies with vastly different working mechanisms and achieved separations. For example, it is very challenging to compare CDI with RO or thermal desalinations using *SEC*, due to the fact that not all technologies can be operated to achieve the same separation. Such a comparison, which may be imperfect yet informative, can be best achieved using *TEE*.

■ ASSOCIATED CONTENT

Supporting Information

The Supporting Information is available free of charge on the ACS Publications website at DOI: 10.1021/acs.est.8b04858.

Summary of the literature data used in constructing Figure 2; data extracted from ref 40; summary of Δg, *SEC* and *TEE* on RO from literature; parameters for simulating Figure 3; interpretation of separation line; illustration of calculation of *TEE* of CDI from literature data; explanation of "flow system limitations"; methodology of simulating potential drops and energy losses in Figure 3; explanation of *TEE* correlation (PDF)

■ AUTHOR INFORMATION

Corresponding Author

*S. Lin. E-mail: shihong.lin@vanderbilt.edu; Tel.: +1 (615) 322-7226.

ORCID

Li Wang: 0000-0002-5542-6696

Shihong Lin: 0000-0001-9832-9127

Notes

The authors declare no competing financial interest.

■ ACKNOWLEDGMENTS

S. Lin acknowledges the support from Oak Ridge Associated Universities (ORAU) through the Ralph E. Powe Jr Faculty Enhancement Award.

■ REFERENCES

(1) Arnold, B. B.; Murphy, G. W. Studies on Electrochemistry of Carbon and Chemically Modified Carbon Surfaces. *J. Phys. Chem.* **1961**, *65* (1), 135−138.

(2) Murphy, G. W.; Caudle, D. D. Mathematical Theory of Electrochemical Demineralization in Flowing Systems. *Electrochim. Acta* **1967**, *12* (12), 1655−1664.

DOI: 10.1021/acs.est.8b04858
Environ. Sci. Technol. 2019, 53, 3366−3378

(3) Ma, J. X.; He, D.; Tang, W. W.; Kovalsky, P.; He, C.; Zhang, C. Y.; Waite, T. D. Development of Redox-Active Flow Electrodes for High-Performance Capacitive Deionization. *Environ. Sci. Technol.* **2016**, *50* (24), 13495−13501.
(4) Peng, Z.; Zhang, D. S.; Shi, L. Y.; Yan, T. T. High performance ordered mesoporous carbon/carbon nanotube composite electrodes for capacitive deionization. *J. Mater. Chem.* **2012**, *22* (14), 6603−6612.
(5) Porada, S.; Weinstein, L.; Dash, R.; van der Wal, A.; Bryjak, M.; Gogotsi, Y.; Biesheuvel, P. M. Water Desalination Using Capacitive Deionization with Microporous Carbon Electrodes. *ACS Appl. Mater. Interfaces* **2012**, *4* (3), 1194−1199.
(6) Wang, H.; Zhang, D. S.; Yan, T. T.; Wen, X. R.; Zhang, J. P.; Shi, L. Y.; Zhong, Q. D. Three-dimensional macroporous graphene architectures as high performance electrodes for capacitive deionization. *J. Mater. Chem. A* **2013**, *1* (38), 11778−11789.
(7) Zhang, D. S.; Yan, T. T.; Shi, L. Y.; Peng, Z.; Wen, X. R.; Zhang, J. P. Enhanced capacitive deionization performance of graphene/carbon nanotube composites. *J. Mater. Chem.* **2012**, *22* (29), 14696−14704.
(8) Kruner, B.; Srimuk, P.; Fleischmann, S.; Zeiger, M.; Schreiber, A.; Aslan, M.; Quade, A.; Presser, V. Hydrogen-treated, submicrometer carbon beads for fast capacitive deionization with high performance stability. *Carbon* **2017**, *117*, 46−54.
(9) Srimuk, P.; Lee, J.; Fleischmann, S.; Choudhury, S.; Jackel, N.; Zeiger, M.; Kim, C.; Aslan, M.; Presser, V. Faradaic deionization of brackish and sea water via pseudocapacitive cation and anion intercalation into few-layered molybdenum disulfide. *J. Mater. Chem. A* **2017**, *5* (30), 15640−15649.
(10) Jain, A.; Kim, J.; Owoseni, O. M.; Weathers, C.; Cana, D.; Zuo, K. C.; Walker, W. S.; Li, Q. L.; Verduzco, R. Aqueous-Processed, High-Capacity Electrodes for Membrane Capacitive Deionization. *Environ. Sci. Technol.* **2018**, *52* (10), 5859−5867.
(11) Tsouris, C.; Mayes, R.; Kiggans, J.; Sharma, K.; Yiacoumi, S.; DePaoli, D.; Dai, S. Mesoporous Carbon for Capacitive Deionization of Saline Water. *Environ. Sci. Technol.* **2011**, *45* (23), 10243−10249.
(12) Li, H. B.; Zou, L. D.; Pan, L. K.; Sun, Z. Novel Graphene-Like Electrodes for Capacitive Deionization. *Environ. Sci. Technol.* **2010**, *44* (22), 8692−8697.
(13) Ahualli, S.; Iglesias, G. R.; Fernandez, M. M.; Jimenez, M. L.; Delgado, A. V. Use of Soft Electrodes in Capacitive Deionization of Solutions. *Environ. Sci. Technol.* **2017**, *51* (9), 5326−5333.
(14) Zhao, R.; Biesheuvel, P. M.; van der Wal, A. Energy consumption and constant current operation in membrane capacitive deionization. *Energy Environ. Sci.* **2012**, *5* (11), 9520−9527.
(15) Omosebi, A.; Gao, X.; Landon, J.; Liu, K. L. Asymmetric Electrode Configuration for Enhanced Membrane Capacitive Deionization. *ACS Appl. Mater. Interfaces* **2014**, *6* (15), 12640−12649.
(16) Porada, S.; Weingarth, D.; Hamelers, H. V. M.; Bryjak, M.; Presser, V.; Biesheuvel, P. M. Carbon flow electrodes for continuous operation of capacitive deionization and capacitive mixing energy generation. *J. Mater. Chem. A* **2014**, *2* (24), 9313−9321.
(17) Hatzell, K. B.; Fan, L.; Beidaghi, M.; Boota, M.; Pomerantseva, E.; Kumbur, E. C.; Gogotsi, Y. Composite Manganese Oxide Percolating Networks As a Suspension Electrode for an Asymmetric Flow Capacitor. *ACS Appl. Mater. Interfaces* **2014**, *6* (11), 8886−8893.
(18) Suss, M. E.; Baumann, T. F.; Bourcier, W. L.; Spadaccini, C. M.; Rose, K. A.; Santiago, J. G.; Stadermann, M. Capacitive desalination with flow-through electrodes. *Energy Environ. Sci.* **2012**, *5* (11), 9511−9519.
(19) Garcia-Quismondo, E.; Santos, C.; Soria, J.; Palma, J.; Anderson, M. A. New Operational Modes to Increase Energy Efficiency in Capacitive Deionization Systems. *Environ. Sci. Technol.* **2016**, *50* (11), 6053−6060.
(20) Kim, C.; Srimuk, P.; Lee, J.; Aslan, M.; Presser, V. Semi-continuous capacitive deionization using multi-channel flow stream and ion exchange membranes. *Desalination* **2018**, *425*, 104−110.
(21) Cho, Y.; Lee, K. S.; Yang, S.; Choi, J.; Park, H. R.; Kim, D. K. A novel three-dimensional desalination system utilizing honeycomb-shaped lattice structures for flow-electrode capacitive deionization. *Energy Environ. Sci.* **2017**, *10* (8), 1746−1750.
(22) Yang, S.; Choi, J.; Yeo, J. G.; Jeon, S. I.; Park, H. R.; Kim, D. K. Flow-Electrode Capacitive Deionization Using an Aqueous Electrolyte with a High Salt Concentration. *Environ. Sci. Technol.* **2016**, *50* (11), 5892−5899.
(23) Gao, X.; Omosebi, A.; Landon, J.; Liu, K. L. Enhanced Salt Removal in an Inverted Capacitive Deionization Cell Using Amine Modified Microporous Carbon Cathodes. *Environ. Sci. Technol.* **2015**, *49* (18), 10920−10926.
(24) He, C.; Ma, J.; Zhang, C.; Song, J.; Waite, T. D. Short-Circuited Closed-Cycle Operation of Flow-Electrode CDI for Brackish Water Softening. *Environ. Sci. Technol.* **2018**, *52* (16), 9350−9360.
(25) Hatzell, K. B.; Hatzell, M. C.; Cook, K. M.; Boota, M.; Housel, G. M.; McBride, A.; Kumbur, E. C.; Gogotsi, Y. Effect of Oxidation of Carbon Material on Suspension Electrodes for Flow Electrode Capacitive Deionization. *Environ. Sci. Technol.* **2015**, *49* (5), 3040−3047.
(26) Gao, X.; Porada, S.; Omosebi, A.; Liu, K. L.; Biesheuvel, P. M.; Landon, J. Complementary surface charge for enhanced capacitive deionization. *Water Res.* **2016**, *92*, 275−282.
(27) Kim, T.; Dykstra, J. E.; Porada, S.; van der Wal, A.; Yoon, J.; Biesheuvel, P. M. Enhanced charge efficiency and reduced energy use in capacitive deionization by increasing the discharge voltage. *J. Colloid Interface Sci.* **2015**, *446*, 317−326.
(28) Porada, S.; Borchardt, L.; Oschatz, M.; Bryjak, M.; Atchison, J. S.; Keesman, K. J.; Kaskel, S.; Biesheuvel, P. M.; Presser, V. Direct prediction of the desalination performance of porous carbon electrodes for capacitive deionization. *Energy Environ. Sci.* **2013**, *6* (12), 3700−3712.
(29) Biesheuvel, P. M.; Hamelers, H. V. M.; Suss, M. E. Theory of Water Desalination by Porous Electrodes with Immobile Chemical Charge. *Colloid Interfac Sci.* **2015**, *9*, 1−5.
(30) Qu, Y. T.; Baumann, T. F.; Santiago, J. G.; Stadermann, M. Characterization of Resistances of a Capacitive Deionization System. *Environ. Sci. Technol.* **2015**, *49* (16), 9699−9706.
(31) Suss, M. E.; Biesheuvel, P. M.; Baumann, T. F.; Stadermann, M.; Santiago, J. G. In Situ Spatially and Temporally Resolved Measurements of Salt Concentration between Charging Porous Electrodes for Desalination by Capacitive Deionization. *Environ. Sci. Technol.* **2014**, *48* (3), 2008−2015.
(32) Biesheuvel, P. M.; Zhao, R.; Porada, S.; van der Wal, A. Theory of membrane capacitive deionization including the effect of the electrode pore space. *J. Colloid Interface Sci.* **2011**, *360* (1), 239−248.
(33) Zhao, R.; Satpradit, O.; Rijnaarts, H. H. M.; Biesheuvel, P. M.; van der Wal, A. Optimization of salt adsorption rate in membrane capacitive deionization. *Water Res.* **2013**, *47* (5), 1941−1952.
(34) Qu, Y. T.; Campbell, P. G.; Hemmatifar, A.; Knipe, J. M.; Loeb, C. K.; Reidy, J. J.; Hubert, M. A.; Stadermann, M.; Santiago, J. G. Charging and Transport Dynamics of a Flow-Through Electrode Capacitive Deionization System. *J. Phys. Chem. B* **2018**, *122* (1), 240−249.
(35) Wang, L.; Lin, S. H. Membrane Capacitive Deionization with Constant Current vs Constant Voltage Charging: Which Is Better? *Environ. Sci. Technol.* **2018**, *52* (7), 4051−4060.
(36) Hemmatifar, A.; Stadermann, M.; Santiago, J. G. Two-Dimensional Porous Electrode Model for Capacitive Deionization. *J. Phys. Chem. C* **2015**, *119* (44), 24681−24694.
(37) Zhao, R.; Porada, S.; Biesheuvel, P. M.; Van der Wal, A. Energy consumption in membrane capacitive deionization for different water recoveries and flow rates, and comparison with reverse osmosis. *Desalination* **2013**, *330*, 35−41.
(38) Anderson, M. A.; Cudero, A. L.; Palma, J. Capacitive deionization as an electrochemical means of saving energy and delivering clean water. Comparison to present desalination practices: Will it compete? *Electrochim. Acta* **2010**, *55* (12), 3845−3856.

DOI: 10.1021/acs.est.8b04858
Environ. Sci. Technol. 2019, 53, 3366−3378

(39) Dlugolecki, P.; van der Wal, A. Energy Recovery in Membrane Capacitive Deionization. *Environ. Sci. Technol.* **2013**, *47* (9), 4904−4910.
(40) Hemmatifar, A.; Ramachandran, A.; Liu, K.; Oyarzun, D. I.; Bazant, M. Z.; Santiago, J. G. Thermodynamics of Ion Separation by Electrosorption. *Environ. Sci. Technol.* **2018**, *52*, 10196−10204.
(41) Porada, S.; Zhao, R.; van der Wal, A.; Presser, V.; Biesheuvel, P. M. Review on the science and technology of water desalination by capacitive deionization. *Prog. Mater. Sci.* **2013**, *58* (8), 1388−1442.
(42) Suss, M. E.; Porada, S.; Sun, X.; Biesheuvel, P. M.; Yoon, J.; Presser, V. Water desalination via capacitive deionization: what is it and what can we expect from it? *Energy Environ. Sci.* **2015**, *8* (8), 2296−2319.
(43) Hawks, S. A.; Ramachandran, A.; Porada, S.; Campbell, P. G.; Suss, M. E.; Biesheuvel, P. M.; Santiago, J. G.; Stadermann, M. Performance Metrics for the Objective Assessment of Capacitive Deionization Systems. *Water Res.* **2019**, *152*, 126−137.
(44) Elimelech, M.; Phillip, W. A. The Future of Seawater Desalination: Energy, Technology, and the Environment. *Science* **2011**, *333* (6043), 712−717.
(45) Fritzmann, C.; Lowenberg, J.; Wintgens, T.; Melin, T. State-of-the-art of reverse osmosis desalination. *Desalination* **2007**, *216* (1−3), 1−76.
(46) Zhao, D. F.; Xue, J. L.; Li, S.; Sun, H.; Zhang, Q. D. Theoretical analyses of thermal and economical aspects of multi-effect distillation desalination dealing with high-salinity wastewater. *Desalination* **2011**, *273* (2−3), 292−298.
(47) Smith, J. M.; Van Ness, H. C.; Abbott, M. M. *Introduction to Chemical Engineering Thermodynamics*, 7th ed.; McGraw-Hil: Boston, MA, 2005.
(48) Lee, J.; Kim, S.; Yoon, J. Rocking Chair Desalination Battery Based on Prussian Blue Electrodes. *Acs Omega* **2017**, *2* (4), 1653−1659.
(49) Pasta, M.; Wessells, C. D.; Cui, Y.; La Mantia, F. A Desalination Battery. *Nano Lett.* **2012**, *12* (2), 839−843.
(50) Bejan, A. *Advanced Engineering Thermodynamics*, 2nd ed.; Wiley: 1997; p 850.
(51) Wang, L.; Biesheuvel, P. M.; Lin, S. Reversible Thermodynamic Cycle Analysis for Capacitive Deionization with Modified Donnan Model. *J. Colloid Interface Sci.* **2018**, *512*, 522−528.
(52) Biesheuvel, P. M. Thermodynamic cycle analysis for capacitive deionization. *J. Colloid Interface Sci.* **2009**, *332* (1), 258−264.
(53) Kang, J.; Kim, T.; Shin, H.; Lee, J.; Ha, J. I.; Yoon, J. Direct energy recovery system for membrane capacitive deionization. *Desalination* **2016**, *398*, 144−150.
(54) Kim, Y. J.; Choi, J. H. Enhanced desalination efficiency in capacitive deionization with an ion-selective membrane. *Sep. Purif. Technol.* **2010**, *71* (1), 70−75.
(55) Lee, J.; Kim, S.; Kim, C.; Yoon, J. Hybrid capacitive deionization to enhance the desalination performance of capacitive techniques. *Energy Environ. Sci.* **2014**, *7* (11), 3683−3689.
(56) Lee, J. H.; Bae, W. S.; Choi, J. H. Electrode reactions and adsorption/desorption performance related to the applied potential in a capacitive deionization process. *Desalination* **2010**, *258* (1−3), 159−163.
(57) Farmer, J. C.; Fix, D. V.; Mack, G. V.; Pekala, R. W.; Poco, J. F. Capacitive deionization of NaCl and NaNO3 solutions with carbon aerogel electrodes. *J. Electrochem. Soc.* **1996**, *143* (1), 159−169.
(58) Kang, J.; Kim, T.; Jo, K.; Yoon, J. Comparison of salt adsorption capacity and energy consumption between constant current and constant voltage operation in capacitive deionization. *Desalination* **2014**, *352*, 52−57.
(59) Kim, S.; Lee, J.; Kim, C.; Yoon, J. Na2FeP2O7 as a Novel Material for Hybrid Capacitive Deionization. *Electrochim. Acta* **2016**, *203*, 265−271.
(60) Liu, Y. H.; Hsi, H. C.; Li, K. C.; Hou, C. H. Electrodeposited Manganese Dioxide/Activated Carbon Composite As a High-Performance Electrode Material for Capacitive Deionization. *ACS Sustainable Chem. Eng.* **2016**, *4* (9), 4762−4770.
(61) Zhao, R.; Biesheuvel, P. M.; Miedema, H.; Bruning, H.; van der Wal, A. Charge Efficiency: A Functional Tool to Probe the Double-Layer Structure Inside of Porous Electrodes and Application in the Modeling of Capacitive Deionization. *J. Phys. Chem. Lett.* **2010**, *1* (1), 205−210.
(62) Biesheuvel, P. M.; van Limpt, B.; van der Wal, A. Dynamic Adsorption/Desorption Process Model for Capacitive Deionization. *J. Phys. Chem. C* **2009**, *113* (14), 5636−5640.
(63) Gao, X.; Omosebi, A.; Landon, J.; Liu, K. L. Surface charge enhanced carbon electrodes for stable and efficient capacitive deionization using inverted adsorption-desorption behavior. *Energy Environ. Sci.* **2015**, *8* (3), 897−909.
(64) Kim, T.; Gorski, C. A.; Logan, B. E. Low Energy Desalination Using Battery Electrode Deionization. *Environ. Sci. Technol. Lett.* **2017**, *4* (10), 444−449.
(65) Choi, S.; Chang, B.; Kim, S.; Lee, J.; Yoon, J.; Choi, J. W. Battery Electrode Materials with Omnivalent Cation Storage for Fast and Charge-Efficient Ion Removal of Asymmetric Capacitive Deionization. *Adv. Funct. Mater.* **2018**, *28*, 1802665.
(66) Shi, W.; Zhou, X.; Li, J.; Meshot, E. R.; Taylor, A. D.; Hu, S.; Kim, J.-H.; Elimelech, M.; Plata, D. L. High-Performance Capacitive Deionization via Manganese Oxide-Coated, Vertically Aligned Carbon Nanotubes. *Environ. Sci. Technol. Lett.* **2018**, *5* (11), 692−700.
(67) Wu, T. T.; Wang, G.; Wang, S. Y.; Zhan, F.; Fu, Y.; Qiao, H. Y.; Qiu, J. S. Highly Stable Hybrid Capacitive Deionization with a MnO2 Anode and a Positively Charged Cathode. *Environ. Sci. Technol. Lett.* **2018**, *5* (2), 98−102.
(68) Hand, S.; Cusick, R. D. Characterizing the Impacts of Deposition Techniques on the Performance of MnO2 Cathodes for Sodium Electrosorption in Hybrid Capacitive Deionization. *Environ. Sci. Technol.* **2017**, *51* (20), 12027−12034.
(69) Chen, F. M.; Huang, Y. X.; Guo, L.; Sun, L. F.; Wang, Y.; Yang, H. Y. Dual-ions electrochemical deionization: a desalination generator. *Energy Environ. Sci.* **2017**, *10* (10), 2081−2089.
(70) Porada, S.; Shrivastava, A.; Bukowska, P.; Biesheuvel, P. M.; Smith, K. C. Nickel Hexacyanoferrate Electrodes for Continuous Cation Intercalation Desalination of Brackish Water. *Electrochim. Acta* **2017**, *255*, 369−378.
(71) Qin, M.; Deshmukh, A.; Epsztein, R.; Patel, S. K.; Owoseni, O. M.; Walker, W. S.; Elimelech, M. Comparison of energy consumption in desalination by capacitive deionization and reverse osmosis. *Desalination* **2019**, *455*, 100−114.
(72) Han, L. C.; Karthikeyan, K. G.; Gregory, K. B. Energy Consumption and Recovery in Capacitive Deionization Using Nanoporous Activated Carbon Electrodes. *J. Electrochem. Soc.* **2015**, *162* (12), E282−E288.
(73) Alkuran, M.; Orabi, M. Utilization of a buck boost converter and the method of segmented capacitors in a CDI water purification system. *2008 12th International Middle East Power System Conference, Vols 1 and 2*; IEEE: New York, 2008.
(74) Dykstra, J. E.; Zhao, R.; Biesheuvel, P. M.; van der Wal, A. Resistance identification and rational process design in Capacitive Deionization. *Water Res.* **2016**, *88*, 358−370.
(75) Hemmatifar, A.; Palko, J. W.; Stadermann, M.; Santiago, J. G. Energy breakdown in capacitive deionization. *Water Res.* **2016**, *104*, 303−311.
(76) Dykstra, J. E.; Porada, S.; van der Wal, A.; Biesheuvel, P. M. Energy consumption in capacitive deionization - Constant current versus constant voltage operation. *Water Res.* **2018**, *143*, 367−375.
(77) Dykstra, J. E. Desalination with porous electrodes: mechanisms of ion transport and adsorption. Dissertation, Wageningen University, Wageningen, The Netherlands, 2018.
(78) Garcia-Quismondo, E.; Gomez, R.; Vaquero, F.; Cudero, A. L.; Palma, J.; Anderson, M. New testing procedures of a capacitive deionization reactor. *Phys. Chem. Chem. Phys.* **2013**, *15* (20), 7648−7656.
(79) Shanbhag, S.; Whitacre, J. F.; Mauter, M. S. The Origins of Low Efficiency in Electrochemical De-Ionization Systems. *J. Electrochem. Soc.* **2016**, *163* (14), E363−E371.

DOI: 10.1021/acs.est.8b04858
Environ. Sci. Technol. 2019, 53, 3366−3378

(80) Zhang, C. Y.; He, D.; Ma, J. X.; Tang, W. W.; Waite, T. D. Faradaic reactions in capacitive deionization (CDI) - problems and possibilities: A review. *Water Res.* **2018**, *128*, 314−330.
(81) Tang, W. W.; He, D.; Zhang, C. Y.; Kovalsky, P.; Waite, T. D. Comparison of Faradaic reactions in capacitive deionization (CDI) and membrane capacitive deionization (MCDI) water treatment processes. *Water Res.* **2017**, *120*, 229−237.
(82) Suss, M. E.; Presser, V. Water Desalination with Energy Storage Electrode Materials. *Joule* **2018**, *2* (1), 10−15.
(83) Hwang, J. Y.; Myung, S. T.; Sun, Y. K. Sodium-ion batteries: present and future. *Chem. Soc. Rev.* **2017**, *46* (12), 3529−3614.
(84) Smith, K. C.; Dmello, R. Na-Ion Desalination (NID) Enabled by Na-Blocking Membranes and Symmetric Na-Intercalation: Porous-Electrode Modeling. *J. Electrochem. Soc.* **2016**, *163* (3), A530−A539.
(85) Smith, K. C. Theoretical evaluation of electrochemical cell architectures using cation intercalation electrodes for desalination. *Electrochim. Acta* **2017**, *230*, 333−341.
(86) Singh, K.; Porada, S.; de Gier, H. D.; Biesheuvel, P. M.; de Smet, L. C. P. M. Timeline on the application of intercalation materials in Capacitive Deionization. *Desalination* **2019**, *455*, 115−134.
(87) Singh, K.; Bouwmeester, H. J. M.; de Smet, L. C. P. M.; Bazant, M. Z.; Biesheuvel, P. M. Theory of Water Desalination with Intercalation Materials. *Phys. Rev. Appl.* **2018**, *9* (6), 064036.
(88) Wei, W. F.; Cui, X. W.; Chen, W. X.; Ivey, D. G. Manganese oxide-based materials as electrochemical supercapacitor electrodes. *Chem. Soc. Rev.* **2011**, *40* (3), 1697−1721.
(89) Li, Q.; Wang, Z. L.; Li, G. R.; Guo, R.; Ding, L. X.; Tong, Y. X. Design and Synthesis of MnO2/Mn/MnO2 Sandwich-Structured Nanotube Arrays with High Supercapacitive Performance for Electrochemical Energy Storage. *Nano Lett.* **2012**, *12* (7), 3803−3807.
(90) West, K.; Jacobsen, T.; Atlung, S. Modeling of Porous Insertion Electrodes with Liquid Electrolyte. *J. Electrochem. Soc.* **1982**, *129* (7), 1480−1485.
(91) Conway, B. E.; Gileadi, E. Kinetic Theory of Pseudo-Capacitance and Electrode Reactions at Appreciable Surface Coverage. *Trans. Faraday Soc.* **1962**, *58* (Dec), 2493−2509.
(92) Zhu, A. H.; Christofides, P. D.; Cohen, Y. Energy Consumption Optimization of Reverse Osmosis Membrane Water Desalination Subject to Feed Salinity Fluctuation. *Ind. Eng. Chem. Res.* **2009**, *48* (21), 9581−9589.
(93) Lin, S. H.; Elimelech, M. Kinetics and energetics trade-off in reverse osmosis desalination with different configurations. *Desalination* **2017**, *401*, 42−52.
(94) Wang, L.; Lin, S. H. Intrinsic tradeoff between kinetic and energetic efficiencies in membrane capacitive deionization. *Water Res.* **2018**, *129*, 394−401.
(95) Cohen, I.; Avraham, E.; Noked, M.; Soffer, A.; Aurbach, D. Enhanced Charge Efficiency in Capacitive Deionization Achieved by Surface-Treated Electrodes and by Means of a Third Electrode. *J. Phys. Chem. C* **2011**, *115* (40), 19856−19863.
(96) Avraham, E.; Noked, M.; Bouhadana, Y.; Soffer, A.; Aurbach, D. Limitations of charge efficiency in capacitive deionization processes III: The behavior of surface oxidized activated carbon electrodes. *Electrochim. Acta* **2010**, *56* (1), 441−447.
(97) Avraham, E.; Noked, M.; Bouhadana, Y.; Soffer, A.; Aurbach, D. Limitations of Charge Efficiency in Capacitive Deionization II. On the Behavior of CDI Cells Comprising Two Activated Carbon Electrodes. *J. Electrochem. Soc.* **2009**, *156* (10), P157−P162.
(98) Gao, X.; Omosebi, A.; Landon, J.; Liu, K. L. Enhancement of charge efficiency for a capacitive deionization cell using carbon xerogel with Modified potential of zero charge. *Electrochem. Commun.* **2014**, *39*, 22−25.
(99) Hawks, S. A.; Knipe, J. M.; Campbell, P. G.; Loeb, C. K.; Hubert, M. A.; Santiago, J. G.; Stadermann, M. Quantifying the flow efficiency in constant-current capacitive deionization. *Water Res.* **2018**, *129*, 327−336.
(100) Johnson, A. M.; Newman, J. Desalting by Means of Porous Carbon Electrodes. *J. Electrochem. Soc.* **1971**, *118* (3), 510−517.

DOI: 10.1021/acs.est.8b04858
Environ. Sci. Technol. 2019, 53, 3366−3378